Dynamic structure factor in impurity-doped spin chains

Annabelle Bohrdt,[1,2] Kevin Jägering,[1] Sebastian Eggert,[1] and Imke Schneider[1]

[1]*Physics Department and Research Center OPTIMAS, University of Kaiserslautern, D-67663 Kaiserslautern, Germany*
[2]*Department of Physics and Institute for Advanced Study, Technical University of Munich, D-85748 Garching, Germany*

The effects of impurities in spin-1/2 Heisenberg chains have recently experienced a renewed interest due to experimental realizations in solid state systems and ultracold gases. Nonmagnetic impurities lead to effectively isolated finite chain segments with a discrete spectrum and characteristic correlations, which have a distinct effect on the dynamic structure factor. Using bosonization and the numerical density matrix renormalization group, we provide detailed quantitative predictions for the momentum- and energy-resolved structure factor in doped systems. Due to the impurities, spectral weight is shifted away from the antiferromagnetic wave vector $k = \pi$ into regions which normally have no spectral weight in the thermodynamic limit. The effect can be quantitatively described in terms of scaling functions, which are derived from a recurrence relation based on bosonization.

Spin chains have been the center of attention as prototypical quantum many-body systems ever since the early days of quantum mechanics [1] and up to this day significant advances have been made, e.g., in describing exact form factors [2–7], exact correlations [8], nonequilibrium states [9,10], and dynamic correlations in the regime of a nonlinear spectrum [11–19]. Recently, there has been renewed experimental interest in doped spin chain systems [20,21] with new results on the Knight shift [22,23], magnetic ordering [24], and the dynamic structure factor [25–28]. The impurities effectively act as missing sites or couplings, which lead to isolated finite chain segments, that are known to acquire characteristic boundary correlation functions [29]. This gives rise to impurity-induced changes in the Knight shift [30–33], the susceptibility [34–37], the static structure factor [31], and the ordering temperature [38,39]. However, surprisingly, a systematic theoretical analysis of the doping effects on the energy- and momentum-resolved dynamic structure factor is still missing. Previous research has taken into account the discrete spectrum of finite chains [25,26,40], which leads to an exponential suppression at low energies. The understanding of the momentum dependence is more involved, however, since characteristic correlations near the impurities play an important role and lead to a strong redistribution of spectral weight to higher momenta outside the two-spinon continuum, as shown in this Rapid Communication.

The underlying model is the well-known *xxz*-spin chain

$$H = J \sum_{i=1}^{L-1} \left(S_i^x S_{i+1}^x + S_i^y S_{i+1}^y + \Delta S_i^z S_{i+1}^z \right), \quad (1)$$

which represents a one-dimensional array of L interacting spin-1/2 operators with *open* boundary conditions. The longitudinal dynamic structure factor is

$$S(\omega,k) = \frac{1}{L} \sum_{j,j'} e^{-ik(j-j')} \int_{-\infty}^{\infty} dt \, e^{i\omega t} \langle S_j^z(t) S_{j'}^z(0) \rangle, \quad (2)$$

which can be measured by angle-resolved neutron scattering experiments [41–43] and gives deep insight into the spatiotemporal correlations. In recent years it was possible to calculate $S(\omega,k)$ from exact methods in the thermodynamic limit [4,5], which is nonzero only within the two-spinon continuum [44], as shown schematically in Fig. 1(b) where the lower threshold is given by $\omega(k) = v|\sin k|$ in terms of the spinon velocity v. Indicated in red are the dominant correlations near the antiferromagnetic wave vector $k = \pi$ at low frequencies, which will be the topic of this Rapid Communication. The low-energy behavior of $S(\omega,k)$ in infinite chains $L \to \infty$ was already predicted in the 1980's using bosonization [45], but it is unclear if this method can be used for finite chains and close to the threshold where the spectral weight is expected to diverge [46]. Such divergences were of great interest in the literature [11–19], where it was shown that a nonlinear dispersion generally leads to qualitative changes of bosonization predictions for dynamical response functions near thresholds. Moreover, even without nonlinear effects, the results become explicitly dependent on the cutoff procedure near those divergent points in quantum wires [47,48].

In this Rapid Communication, a finite-size formulation of bosonization is used, which gives surprisingly accurate results compared to density matrix renormalization group (DMRG) simulations even directly at the thresholds, without the need for any fitting parameters, cutoff procedures, or nonlinear corrections. We explicitly estimate the range of the low-energy region where the results are valid. Our finite-size method leads to a recursion, which gives a closed *analytic* expression of the k-dependent structure factor for any energy, length, and anisotropy Δ. We observe a distinct broadening at the threshold, which is not due to nonlinear effects, but is a direct result of the open boundary conditions. Accordingly, in doped systems, a characteristic transfer of spectral weight occurs from the two-spinon continuum into regions where no signal would be expected for undoped chains. It is possible to extrapolate our results to the thermodynamic limit [49],

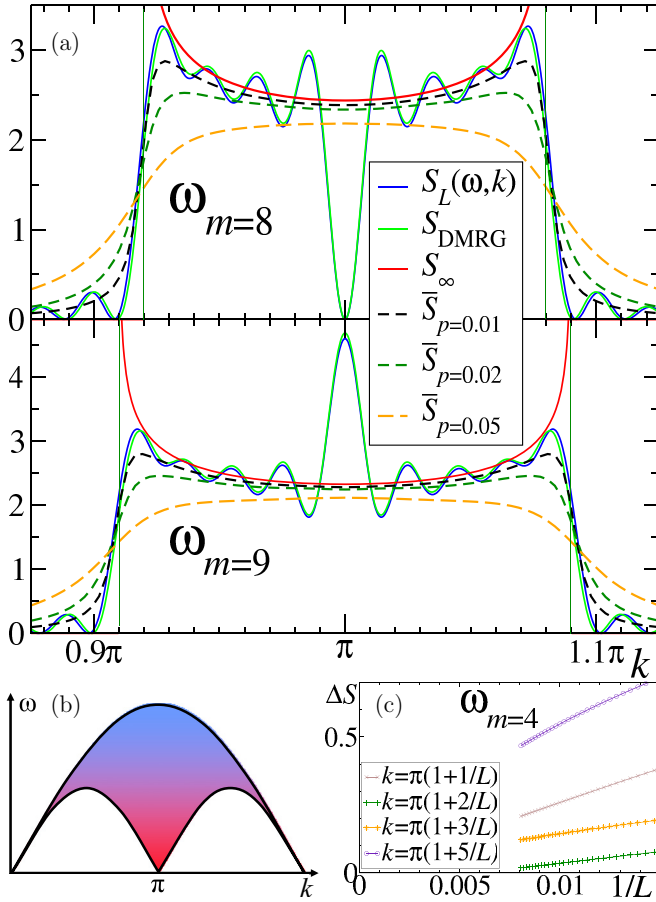$$S_\infty(\omega,k) = (2v)^{1-2K} \pi^2 A_z \Gamma^{-2}(K) [\omega^2 - \omega^2(k)]^{K-1}, \quad (3)$$

FIG. 1. (a) The dynamical structure factor $S_L(\omega_m,k)$ at $L = 100$ as a function of k near π from bosonization compared to numerical DMRG calculations for $\omega_m = 8\frac{\pi v}{L} \approx 0.31J$ and $9\frac{\pi v}{L} \approx 0.348J$. The $L \to \infty$ behavior S_∞ from Eq. (3) and the averaged signal $\bar{S}_p$ with doping level p at the same energies are also shown where vertical lines mark $v|k - \pi| \approx \omega_m$. (b) Schematic two-spinon continuum. (c) Bosonization error over finite-size deviation ΔS in Eq. (14) for $m = 4$ and different k using $K = 0.8$ as a function of $1/L$.

for $\omega(k) < \omega$ near $k \approx \pi$, where $K = \pi/2(\pi - \theta)$ is the Luttinger parameter and $v = J\pi \sin\theta/2\theta$ in terms of $\cos\theta = \Delta$ [50]. The overall amplitude A_z is known from exact methods [51]. Since $K < 1$ for $\Delta > 0$, the signal increases with ω^{2K-2} as the frequency is lowered and shows a divergence near the threshold $\omega - \omega(k) \to 0^+$, but vanishes for $\omega(k) > \omega$. This behavior agrees with bosonization in the thermodynamic limit [45], and nonlinear effects do *not* change the exponent near the threshold due to the high symmetry at zero magnetic field, as was shown by the Bethe ansatz [15].

Bosonization methods and therefore also Eq. (3) are low-energy approximations. Using a finite-size approach, we are able to quantitatively estimate the region of validity in comparison with our DMRG results, by demanding that all many-body energy excitations can be grouped into nearly degenerate well-separated levels m such that higher-order corrections [29,52–55] are smaller than the level spacing, as described in the Supplemental Material [49]. We find that the spectrum is well described by equally spaced energy levels $\omega_m \approx m\Delta\omega$ with $\Delta\omega = \frac{\pi v}{L}$ as long as $\omega_m < \omega_c$, where the cutoff frequency

$\omega_c(K = 0.5) \approx 0.2J$, $\omega_c(K = 0.6) \approx 0.5J$, $\omega_c(K \geqslant 0.7) \approx J$ is dependent on anisotropy, but valid for all lengths [49].

Because of the discrete spectrum, Eq. (2) can then be expressed in the Lehmann representation

$$S(\omega,k) = \Delta\omega \sum_{m\neq 0} S_L(\omega_m,k)\delta(\omega - \omega_m), \qquad (4)$$

where we have defined individual spectral weights,

$$S_L(\omega_m,k) = \frac{2\pi}{\Delta\omega}\left|\langle\omega_m|S_k^z|0\rangle\right|^2, \qquad (5)$$

with $S_k^z = \frac{1}{\sqrt{L}}\sum_j e^{-ikj}S_j^z$ and a sum over nearly degenerate states in each level is implied. Note that the scattering wave vectors k are not quantized.

Numerically, we implemented a DMRG code [56] using the multitargeting algorithm for spectral weights [57,58] in order to obtain the first 97 excitations, which captures all nearly degenerate multiplets up to energy level $m = 9$ corresponding to realistic experimental energy and length scales. Typical results for $S_L(\omega_m,k)$ are shown in Fig. 1(a). Using $M = 600$ DMRG states gives an accuracy in the wave function of order 10^{-2} relative to exact results from the xx model.

Analytically, we use a finite-size formulation of bosonization [29,39,53,59,60] as reviewed in the Supplemental Material [49], which is based on expressing the alternating part of the spin operator using a free bosonic field ϕ,

$$S^z(x,t) \approx A(-1)^x \sin\sqrt{4\pi K}\phi(x,t), \qquad (6)$$

where the amplitude $A^2 = A_z/2$ is known from exact methods [51]. Long-distance correlations can then be calculated by expectation values of the form

$$G^\pm(x,y,t) = \langle e^{i\sqrt{4\pi K}\phi(x,t)}e^{\mp i\sqrt{4\pi K}\phi(y,0)}\rangle. \qquad (7)$$

The main technical difficulty is the Fourier transform over time in Eq. (2), which ordinarily requires a detailed analysis of the analytic structure and contour integrals with a cutoff procedure [45,46,61]. However, in our calculation we use finite systems, which provides an efficient way of calculating spectral weights, that can be summarized in a few lines as follows. Due to the discrete energy spectrum, the Fourier transform gives a sum over delta functions,

$$\int_{-\infty}^\infty dt\, G^\pm(x,y,t)e^{i\omega t} = 2\pi\sum_m S_m^\pm(x,y)\delta(\omega - \omega_m). \qquad (8)$$

To evaluate the spectral weights $S_m^\pm$ it is possible to use the mode expansion and an integration by parts of Eq. (8) to arrive at a recurrence relation [49,62,63],

$$S_m^\pm(x,y) = \frac{\pm 1}{m}\sum_{\ell=1}^m S_{m-\ell}^\pm(x,y)\,\gamma_\ell(x,y), \qquad (9)$$

which allows us to express the $S_m^\pm$ in Eq. (8) as a recursive sum of the ones with lower index $m - \ell$ using starting values of

$$S_0^+(x,y) = S_0^-(x,y) = c(x)c(y)$$

$$= \left(\frac{4L^2}{\pi^2}\sin\frac{\pi x}{L}\sin\frac{\pi y}{L}\right)^{-K}, \qquad (10)$$

and the coefficients

$$\gamma_\ell(x,y) = 4K \sin \frac{\ell \pi x}{L} \sin \frac{\ell \pi y}{L}. \tag{11}$$

It is then straightforward to evaluate the spatial Fourier transform

$$S_m^\pm(k) = \frac{1}{L} \int_0^L dx \int_0^L dy \, e^{i(\pi-k)(x-y)} S_m^\pm(x,y), \tag{12}$$

to obtain the spectral weights S_L in Eq. (5),

$$S_L(\omega_m, k) = \frac{A_z L}{2v}[S_m^+(k) - S_m^-(k)]. \tag{13}$$

In the case of odd L the integrands $S_m^\pm(x,y)$ acquire an additional factor of $\cos \pi(x \pm y)/L$ from zero modes, which reflects the parity symmetries of the wave functions [49]. Note that the spatial Fourier transform in Eq. (12) dominates for antiferromagnetic wave vectors $k \approx \pi$, i.e., small $q = k - \pi$. The expression for $S_m^\pm(x,y)$ from Eq. (9) contains products of different γ_ℓ with the starting value $S_0^\pm$, so the spatial integral in Eq. (12) can be evaluated exactly [49]. For any level m and length L, we therefore quickly arrive at a finite sum of terms for $S_L(\omega_m, k)$ which provides the dependence on k analytically.

A direct comparison between bosonization S_L and numerics S_{DMRG} is shown in Fig. 1(a) for energy levels $m = 8$ and $m = 9$ in a finite system of $L = 100$ with $K = 0.8$. Without any fit, the agreement is surprisingly accurate and even captures details such as an alternating signal at $k = \pi$ with even and odd m due to parity symmetry, which leads to overall oscillations. Due to the zero-mode prefactor [49] the same alternation is observed between even and odd lengths L. For a quantitative analysis we further compare the small error between DMRG S_{DMRG} and bosonization S_L with the finite-size correction relative to the bulk behavior S_∞ in Eq. (3) by defining

$$\Delta S \equiv \frac{S_L - S_{\text{DMRG}}}{S_L - S_\infty}. \tag{14}$$

Both the numerator and the denominator go to zero as $L \to \infty$, but the error to the numerics vanishes more quickly with $1/L$ as shown in Fig. 1(c) for $m = 4$, $K = 0.8$, and selected k values, for which the denominator tends to be small.

We are now in the position to efficiently calculate S_L for a large range of L, k, and ω_m to average the signal in a randomly doped system. An impurity density p of nonmagnetic sites gives a distribution of chain lengths [39,40,64] $P(L) = p^2(1-p)^L$ normalized so that $\sum L P(L) = 1 - p$. The averaged signal $\bar{S}_p$ for typical experimental doping values in Fig. 1(a) shows that the signal at the divergence is strongly reduced relative to the undoped case $L \to \infty$ while significant spectral weight is observed just outside the two-spinon continuum $\omega(q) \approx |vq| > \omega$ for $q = k - \pi$.

It must be emphasized that the finite-size bosonization is completely divergence free. For any finite or impurity-doped system we obtain a well-behaved finite signal even at $\omega(q) = \omega$, in agreement with DMRG. Nonetheless, it is interesting to start from the thermodynamic limit in Eq. (3) and consider a finite-size expansion in $1/L$,

$$S_L(\omega, k) = S_\infty(\omega, k) + L^{-1} S_{\text{imp}}(\omega, k) + O(L^{-2}), \tag{15}$$

which defines an impurity correction S_{imp} [31]. Based on the efficient calculation of spectral weights from Eqs. (9)–(13),
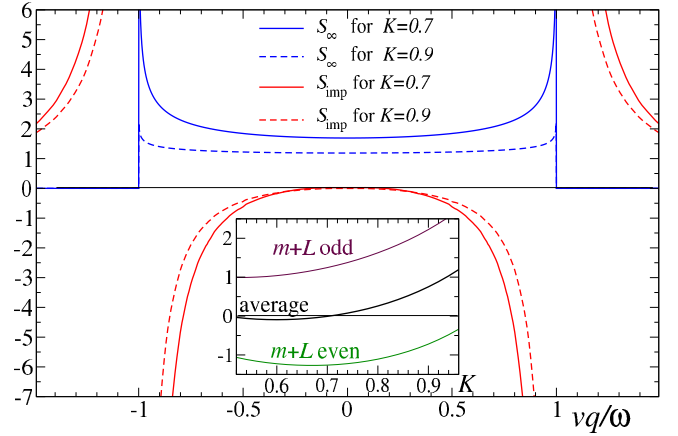

FIG. 2. The rescaled signal $(\frac{\omega}{v})^{2-2K} S_\infty$ and $(\frac{\omega}{v})^{3-2K} S_{\text{imp}}$ as functions of the scaling variable vq/ω for $K = 0.7$ and $K = 0.9$. Inset: Relative impurity contribution $\omega \widehat{S}_{\text{imp}}(\omega)/v \widehat{S}_\infty(\omega)$ from the k-integrated signal as a function of K.

we can make a comprehensive finite-size scaling to determine S_∞ and S_{imp} for different ω and k. Due to the scale invariance of the underlying bosonization the resulting contributions in Eq. (15) show perfect data collapse, so that $\omega^{2-2K} S_\infty$ and $\omega^{3-2K} S_{\text{imp}}$ are only functions of the scaling variable vq/ω, as shown in Fig. 2 for $K = 0.7$ and $K = 0.9$. While S_∞ is given by Eq. (3), we find that $S_{\text{imp}} \propto \omega^{2K-3}$ increases even faster with decreasing ω. This is reminiscent of quantum wires, which also show boundary-dominated spectral functions at low energies [61]. Even more interesting is the strong divergence of the impurity part in Fig. 2, which goes as $||vq| - \omega|^{K-2}$ and implies a breakdown of the $1/L$ expansion in Eq. (15) as $|vq| \to \omega$. This breakdown is not due to nonlinear effects or higher-order operators, but implies a cancellation of larger and larger contributions in the expansion Eq. (15) as $|vq| \to \omega$, which is counterproductive to obtain a *finite* result at finite L. Therefore, bosonization for finite systems actually works better in this case than in the thermodynamic limit.

Nonetheless, the expansion in Eq. (15) is useful away from the divergences in order to estimate the length-averaged signal to lowest order in p,

$$\bar{S}_p(\omega, k) \approx E_1\left(\frac{p\pi v}{\omega}\right) S_\infty(\omega, k) + p E_2\left(\frac{p\pi v}{\omega}\right) S_{\text{imp}}(\omega, k), \tag{16}$$

in terms of the Einstein functions E_1 and E_2,

$$E_1(x) = \frac{x^2 e^x}{(e^x - 1)^2} \quad \text{and} \quad E_2(x) = \frac{x}{e^x - 1}, \tag{17}$$

that are derived in the Supplemental Material [49]. The rescaled average $\omega^{2-2K} \bar{S}_p$ in Eq. (16) is now a function of two scaling variables vq/ω and vp/ω. The corresponding data collapse holds approximately also for the averages over all lengths shown in Fig. 1(a) above, so that the signal for a given ω can easily be generalized to other energies. Both E_1 and E_2 become exponentially small for energies below the average-length gap $\omega \ll \pi v/\bar{L} \equiv p\pi v$. The suppression of bulk spectral weight with E_1 due to the finite-size gaps was discussed and observed

experimentally [25,26], but we find that the additional redistribution of spectral weight becomes very important, which can be traced to the effect of boundary correlations.

The averaged signal in Fig. 1(a) and the impurity correction in Fig. 2 show that the signal is strongly reduced for $|vq| < \omega$, while spectral weight is created for $|vq| > \omega$. This invites the question if the k-integrated signal $\widehat{S}(\omega)$ at a given energy is overall increased or decreased or even unchanged due to the boundaries. This is relevant for neutron scattering experiments, which recently observed significant changes of the spectral weight around $k \approx \pi$ depending on the doping [27,28]. To calculate the integrated antiferromagnetic spectral weight $\widehat{S}$ as a function of L, we use the fact that an integration over k of Eq. (12) leads to a delta function $2\pi\delta(x - y)$, so it is possible to apply the recurrence relation in Eq. (9) for $S_m^{\pm}(x, x)$, which is inserted into the corresponding spatial integral. Finite-size scaling gives a bulk part $\widehat{S}_{\infty}(\omega) \propto \omega^{2K-1}$ which now decreases with decreasing ω corresponding to the integral of Eq. (3). However, the impurity part $\widehat{S}_{\mathrm{imp}}(\omega) \propto \omega^{2K-2}$ increases with decreasing ω, so we define the energy-independent ratio $\omega\widehat{S}_{\mathrm{imp}}(\omega)/v\widehat{S}_{\infty}(\omega)$, which is only dependent on K (i.e., Δ), as shown in the inset of Fig. 2. Note that due to the alternation with m and L the impurity part is different if $m + L$ is even or odd, but the experimentally relevant average gives a finite and relatively small value. Therefore, the corresponding expansion and averaging in Eqs. (15) and (16) work well to calculate the doping and energy dependence using the k-integrated data in Fig. 2 (inset). The impurity part becomes negative at $K \lesssim 0.7$, i.e., larger Δ, which may in part explain an additional depletion of spectral weight at low energies, but the experimentally observed changes with different impurity types [27] require more refined models beyond simple chain breaks.

Last but not least, it is instructive to consider finite systems with periodic boundary conditions. The starting values in Eq. (10) are now independent of position $c = \left(\frac{2\pi}{L}\right)^K$, so all integrals can be done directly and the recurrence relation leads to an analytical result for all energies, lengths, and momenta [49],

$$S_L(\omega_m, k_l) = \frac{A_z L^2 c^2}{4v\Gamma^2(K)} \frac{\Gamma\left(\frac{m+l}{2} + K\right)}{\Gamma\left(\frac{m+l}{2} + 1\right)} \frac{\Gamma\left(\frac{m-l}{2} + K\right)}{\Gamma\left(\frac{m-l}{2} + 1\right)}, \quad (18)$$

where now $\omega_m = 2\pi vm/L$ and also $k_l - \pi = 2\pi l/L$ is quantized due to periodicity with the condition that l and m are either both even or both odd integers and $|l| \leqslant m$. Therefore, there is no spectral weight for $v|k_l - \pi| > \omega_m$, in strong contrast to the open boundary conditions discussed above. It is straightforward to expand Eq. (18) in $1/L$ using Stirling's formula [49] to obtain S_{∞} in Eq. (3) and a negative impurity part S_{imp}.

In summary, we have analyzed the structure factor of doped spin chain systems. Using bosonization and numerical DMRG, we see that doping leads to a significant shift of spectral weight from $k \approx \pi$ to regions $v|k - \pi| > \omega$ in neutron scattering experiments, which would not show any signal for infinite or periodic systems. The relative change from doping near the threshold $|vq| \to \omega$ is infinitely large, so that the first-order impurity contribution diverges near the threshold $\omega(q)$ with a stronger power law than the bulk and a $1/L$ expansion from the thermodynamic limit always breaks down. Previous studies also found that the divergence in the thermodynamic limit is not universal, but instead is strongly dependent on either the cutoff procedure [47,48] or higher-order terms. Naively, it could have been expected that bosonization works particularly well in the thermodynamic limit, but instead it turns out that the finite-size theory is much better controlled and quantitatively accurate even for $|vq| \to \omega$, as shown in Fig. 1. From a technical point of view, the mode expansion for finite systems leads to finite sums, which can be efficiently evaluated to a closed analytical expression using a recurrence relation without the need for contour integral, asymptotic limits, nonlinearities, or cutoff procedures.

It is fair to say that in one dimension it is always important to consider boundaries, since physical systems only contain finite chains even in the absence of doping [65]. This is especially also true for artificially created spin chains using surface structures [66,67], ion traps [68], or ultracold gases [69–72] as quantum simulators, where measurements of energy- and space-resolved correlations are in principle possible [73].

Finally, we would also like to discuss the limitations and open questions which remain. In the limit $\Delta \to 1$ it is well known that logarithmic corrections lead to strong quantitative changes [52]. Those log corrections have not yet been fully understood for open boundary systems [53,60] and are beyond the scope of this Rapid Communication. Nonetheless, the DMRG analyses for $K = 0.7$ and $K = 0.6$ (larger Δ) show that the predicted momentum dependence is not strongly changed by higher-order operators. Instead, we observe an overall renormalization of the signal with a k-independent factor of the form $(1 - 0.26\omega^{\gamma}/\gamma)$ with $\gamma = 4K - 2$, as argued in the Supplemental Material [49]. For future research it would be interesting to look for the corresponding renormalization in periodic chains, where the structure factor can be calculated exactly [2–7]. In any case, the strong transfer of spectral weight to $v|k - \pi| > \omega$ for open chains is a robust feature even for $\Delta = 1$.

[1] H. Bethe, Zur Theorie der Metalle, Z. Phys. A **71**, 205 (1931).

[2] J.-S. Caux and J. M. Maillet, Computation of Dynamical Correlation Functions of Heisenberg Chains in a Magnetic Field, Phys. Rev. Lett. **95**, 077201 (2005).

[3] J.-S. Caux, R. Hagemans, and J. M. Maillet, Computation of dynamical correlation functions of Heisenberg chains: The gapless anisotropic regime, J. Stat. Mech. (2005) P09003.

[4] J.-S. Caux, H. Konno, M. Sorrell, and R. Weston, Tracking the Effects of Interactions on Spinons in Gapless Heisenberg Chains, Phys. Rev. Lett. **106**, 217203 (2011).

[5] J.-S. Caux, H. Konno, M. Sorrell, and R. Weston, Exact form-factor results for the longitudinal structure factor of the massless XXZ model in zero field, J. Stat. Mech. (2012) P01007.

[6] A. Shashi, M. Panfil, J.-S. Caux, and A. Imambekov, Exact prefactors in static and dynamic correlation functions of one-dimensional quantum integrable models: Applications to the Calogero-Sutherland, Lieb-Liniger, and XXZ models, Phys. Rev. B **85**, 155136 (2012).

[7] N. Kitanine, K. K. Kozlowski, J. M. Maillet, N. A. Slavnov, and V. Terras, Form factor approach to dynamical correlation functions in critical models, J. Stat. Mech. (2012) P09001.

[8] M. Dugave, F. Göhmann, and K. K. Kozlowski, Low-temperature large-distance asymptotics of the transversal two-point functions of the XXZ chain, J. Stat. Mech. (2014) P04012.

[9] T. Prosen and M. Znidaric, Matrix product simulations of non-equilibrium steady states of quantum spin chains, J. Stat. Mech. (2009) P02035.

[10] A. De Luca, M. Collura, and J. De Nardis, Nonequilibrium spin transport in integrable spin chains: Persistent currents and emergence of magnetic domains, Phys. Rev. B **96**, 020403(R) (2017).

[11] A. Imambekov and L. I. Glazman, Universal theory of nonlinear Luttinger liquids, Science **323**, 228 (2009).

[12] L. I. Glazman, A. Imambekov, and T. L. Schmidt, One-dimensional quantum liquids: Beyond the Luttinger liquid paradigm, Rev. Mod. Phys. **84**, 1253 (2012).

[13] R. G. Pereira, J. Sirker, J.-S. Caux, R. Hagemans, J. M. Maillet, S. R. White, and I. Affleck, Dynamical Spin Structure Factor for the Anisotropic Spin-1/2 Heisenberg Chain, Phys. Rev. Lett. **96**, 257202 (2006).

[14] R. G. Pereira, J. Sirker, J.-S. Caux, R. Hagemans, J. M. Maillet, S. R. White, and I. Affleck, Dynamical structure factor at small q for the XXZ spin-1/2 chain, J. Stat. Mech. (2007) P08022.

[15] R. G. Pereira, S. R. White, and I. Affleck, Exact Edge Singularities and Dynamical Correlations in Spin-1/2 Chains, Phys. Rev. Lett. **100**, 027206 (2008).

[16] V. Cheianov and M. Pustilnik, Threshold Singularities in the Dynamic Response of Gapless Integrable Models, Phys. Rev. Lett. **100**, 126403 (2008).

[17] C. Karrasch, R. G. Pereira, and J. Sirker, Low temperature dynamics of nonlinear Luttinger liquids, New J. Phys. **17**, 103003 (2015).

[18] I. S. Eliens, F. B. Ramos, J. C. Xavier, and R. G. Pereira, Boundary versus bulk behavior of time-dependent correlation functions in one-dimensional quantum systems, Phys. Rev. B **93**, 195129 (2016).

[19] H. Karimi and I. Affleck, Transverse spectral functions and Dzyaloshinskii-Moriya interactions in XXZ spin chains, Phys. Rev B **84**, 174420 (2011).

[20] K. Karmakar and S. Singh, Finite-size effects in the quasi-one-dimensional quantum magnets Sr_2CuO_3, $Sr_2Cu_{0.99}M_{0.01}O_3$ (M = Ni, Zn), and $SrCuO_2$, Phys. Rev. B **91**, 224401 (2015).

[21] F. Hammerath, E. M. Brüning, S. Sanna, Y. Utz, N. S. Beesetty, R. Saint-Martin, A. Revcolevschi, C. Hess, B. Büchner, and H.-J. Grafe, Spin gap in the single spin-1/2 chain cuprate $Sr_{1.9}Ca_{0.1}CuO_3$, Phys. Rev. B **89**, 184410 (2014).

[22] Y. Utz *et al.*, Effect of different in-chain impurities on the magnetic properties of the spin chain compound $SrCuO_2$ probed by NMR, Phys. Rev. B **96**, 115135 (2017).

[23] Y. Utz, F. Hammerath, S. Nishimoto, C. Hess, N. S. Beesetty, R. Saint-Martin, A. Revcolevschi, B. Buchner, and H. J. Grafe, Suppression of the impurity-induced local magnetism by the opening of a spin pseudogap in Ni-doped Sr_2CuO_3, Phys. Rev. B **92**, 060405 (2015).

[24] G. Simutis *et al.*, Magnetic ordering in the ultrapure site-diluted spin chain materials $SrCu_{1-x}Ni_xO_2$, Phys. Rev. B **93**, 214430 (2016).

[25] G. Simutis *et al.*, Spin Pseudogap in Ni-Doped $SrCuO_2$, Phys. Rev. Lett. **111**, 067204 (2013).

[26] G. Simutis *et al.*, Spin pseudogap in the $S = 1/2$ chain material Sr_2CuO_3 with impurities, Phys. Rev. B **95**, 054409 (2017).

[27] K. Karmakar, M. Skoulatos, G. Prando, B. Roessli, U. Stuhr, F. Hammerath, C. Rüegg, and S. Singh, Effects of Quantum Spin-1/2 Impurities on the Magnetic Properties of Zigzag Spin Chains, Phys. Rev. Lett. **118**, 107201 (2017).

[28] K. Karmakar, R. Bag, M. Skoulatos, C. Rüegg, and S. Singh, Impurities in the weakly coupled quantum spin chains Sr_2CuO_3 and $SrCuO_2$, Phys. Rev. B **95**, 235154 (2017).

[29] S. Eggert and I. Affleck, Magnetic impurities in half-integer Heisenberg antiferromagnetic chains, Phys. Rev. B **46**, 10866 (1992).

[30] J. Sirker and N. Laflorencie, NMR response in quasi-one-dimensional spin-1/2 antiferromagnets, Europhys. Lett. **86**, 57004 (2009).

[31] S. Eggert and I. Affleck, Impurities in $S = 1/2$ Heisenberg Antiferromagnetic Chains: Consequences for Neutron Scattering and Knight Shift, Phys. Rev. Lett. **75**, 934 (1995).

[32] S. Eggert and S. Rommer, Universal Crossover Behavior of a Magnetic Impurity and Consequences for Doping in Spin-1/2 Chains, Phys. Rev. Lett. **81**, 1690 (1998).

[33] S. Rommer and S. Eggert, Spin- and charge-density oscillations in spin chains and quantum wires, Phys. Rev. B **62**, 4370 (2000).

[34] S. Fujimoto and S. Eggert, Boundary Susceptibility in the Spin-1/2 Chain: Curie-Like Behavior without Magnetic Impurities, Phys. Rev. Lett. **92**, 037206 (2004).

[35] J. Sirker, N. Laflorencie, S. Fujimoto, S. Eggert, and I. Affleck, Chain Breaks and the Susceptibility of $Sr_2Cu_{1-x}Pd_xO_{3+d}$ and Other Doped Quasi-One-Dimensional Antiferromagnets, Phys. Rev. Lett. **98**, 137205 (2007).

[36] J. Sirker, S. Fujimoto, N. Laflorencie, S. Eggert, and I. Affleck, Thermodynamics of impurities in the anisotropic Heisenberg spin-1/2 chain, J. Stat. Mech. (2008) P02015.

[37] S. Rommer and S. Eggert, Impurity corrections to the thermodynamics in spin-1/2 chains using a transfer-matrix DMRG method, Phys. Rev. B **59**, 6301 (1999).

[38] K. M. Kojima *et al.*, Reduction of Ordered Moment and Néel Temperature of Quasi-One-Dimensional Antiferromagnets Sr_2CuO_3 and Ca_2CuO_3, Phys. Rev. Lett. **78**, 1787 (1997).

[39] S. Eggert, I. Affleck, and M. D. P. Horton, Néel Order in Doped Quasi-One-Dimensional Antiferromagnets, Phys. Rev. Lett. **89**, 047202 (2002).

[40] S. Wessel and S. Haas, Excitation spectra and thermodynamic response of segmented Heisenberg spin chains, Phys. Rev. B **61**, 15262 (2000).

[41] B. Lake, D. A. Tennant, C. D. Frost, and S. E. Nagler, Quantum criticality and universal scaling of a quantum antiferromagnet, Nat. Mater. **4**, 329 (2005).

[42] B. Lake, D. A. Tennant, and S. E. Nagler, Longitudinal magnetic dynamics and dimensional crossover in the quasi-one-dimensional spin-1/2 Heisenberg antiferromagnet $KCuF_3$, Phys. Rev. B **71**, 134412 (2005).

[43] B. Lake, D. A. Tennant, J.-S. Caux, T. Barthel, U. Schollwöck, S. E. Nagler, and C. D. Frost, Multispinon Continua at Zero and Finite Temperature in a Near-Ideal Heisenberg Chain, Phys. Rev. Lett. **111**, 137205 (2013).

[44] J. des Cloizeaux and J. J. Pearson, Spin-wave spectrum of the antiferromagnetic linear chain, Phys. Rev. **128**, 2131 (1962).

[45] H. J. Schulz, Phase diagrams and correlation exponents for quantum spin chains of arbitrary spin quantum number, Phys. Rev. B **34**, 6372 (1986).

[46] V. Meden and K. Schönhammer, Spectral functions for the Tomonaga-Luttinger model, Phys. Rev. B **46**, 15753 (1992).

[47] V. Meden, Nonuniversality of the one-particle Green's function of a Luttinger liquid, Phys. Rev. B **60**, 4571 (1999).

[48] L. Markhof and V. Meden, Spectral function of the Tomonaga-Luttinger model revisited: Power laws and universality, Phys. Rev. B **93**, 085108 (2016).

[49] See Supplemental Material at http://link.aps.org/supplemental/10.1103/PhysRevB.98.020402 for a derivation of the energy range of validity, correlation functions, recurrence equation, exact integrals, rescaling at smaller K, periodic boundary conditions, and averaging.

[50] For a review on bosonization, see T. Giamarchi, *Quantum Physics in One Dimension* (Oxford University Press, Oxford, U.K., 2003).

[51] S. Lukyanov and V. Terras, Long-distance asymptotics of spin-spin correlation functions for the XXZ spin chain, Nucl. Phys. B **654**, 323 (2003).

[52] I. Affleck, D. Gepner, H. J. Schulz, and T. Ziman, Critical behaviour of spin-s Heisenberg antiferromagnetic chains: analytic and numerical results, J. Phys. A: Math. Gen. **22**, 511 (1989).

[53] J. Sirker and M. Bortz, The open XXZ-chain: Bosonisation, the Bethe ansatz, and logarithmic corrections, J. Stat. Mech. (2006) P01007.

[54] M. Bortz, M. Karbach, I. Schneider, and S. Eggert, Lattice versus continuum theory of the periodic Heisenberg chain, Phys. Rev. B **79**, 245414 (2009).

[55] J. L. Cardy, Operator content of two-dimensional conformally invariant theories, Nucl. Phys. B **270**, 186 (1986).

[56] S. R. White, Density Matrix Formulation for Quantum Renormalization Groups, Phys. Rev. Lett. **69**, 2863 (1992); Density-matrix algorithms for quantum renormalization groups, Phys. Rev. B **48**, 10345 (1993).

[57] I. Schneider, A. Struck, M. Bortz and S. Eggert, Local Density of States for Individual Energy Levels in Finite Quantum Wires, Phys. Rev. Lett. **101**, 206401 (2008)

[58] S. A. Söffing, I. Schneider, and S. Eggert, Low-energy local density of states of the 1D Hubbard model, Europhys. Lett. **101**, 56006 (2013).

[59] A. E. Mattsson, S. Eggert, and H. Johannesson, Properties of a Luttinger liquid with boundaries at finite temperature and size, Phys. Rev. B **56**, 15615 (1997).

[60] I. Affleck and S. Qin, Logarithmic corrections in quantum impurity problems, J. Phys. A **32**, 7815 (1999).

[61] S. Eggert, H. Johannesson, and A. Mattsson, Boundary Effects on Spectral Properties of Interacting Electrons in One Dimension, Phys. Rev. Lett. **76**, 1505 (1996).

[62] K. Schönhammer and V. Meden, Nonuniversal spectral properties of the Luttinger liquid, Phys. Rev. B **47**, 16205 (1993).

[63] I. Schneider and S. Eggert, Recursive Method for the Density of States in One Dimension, Phys. Rev. Lett. **104**, 036402 (2010).

[64] D. Stauffer and C. Jayaprakash, Critical exponents for one-dimensional percolation clusters, Phys. Lett. A **64**, 433 (1978).

[65] M. Takigawa, N. Motoyama, H. Eisaki, and S. Uchida, Field-induced staggered magnetization near impurities in the $S = 1/2$ one-dimensional Heisenberg antiferromagnet Sr_2CuO_3, Phys. Rev. B **55**, 14129 (1997).

[66] X. Chen, Y.S. Fu, S.H. Ji, T. Zhang, P. Cheng, X.C. Ma, X.L. Zou, W.H. Duan, J.F. Jia, and Q.K. Xue, Probing Superexchange Interaction in Molecular Magnets by Spin-Flip Spectroscopy and Microscopy, Phys. Rev. Lett. **101**, 197208 (2008).

[67] C. F. Hirjibehedin, C. P. Lutz, and A. J. Heinrich, Spin coupling in engineered atomic structures, Science **312**, 1021 (2006).

[68] D. Porras and J. I. Cirac, Effective Quantum Spin Systems with Trapped Ions, Phys. Rev. Lett. **92**, 207901 (2004).

[69] B. Schmidt, M. Bortz, S. Eggert, M. Fleischhauer, and D. Petrosyan, Attractively bound pairs of atoms in the Bose-Hubbard model and antiferromagnetism, Phys. Rev. A **79**, 063634 (2009).

[70] T. A. Hilker, G. Salomon, F. Grusdt, A. Omran, M. Boll, E. Demler, I. Bloch, and C. Gross, Revealing hidden antiferromagnetic correlations in doped Hubbard chains via string correlators, Science **357**, 484 (2017).

[71] A. Vogler, R. Labouvie, G. Barontini, S. Eggert, V. Guarrera, and H. Ott, Dimensional Phase Transition From An Array of 1D Luttinger Liquids to a 3D Bose-Einstein Condensate, Phys. Rev. Lett. **113**, 215301 (2014).

[72] A. Mazurenko, C. S. Chiu, G. Ji, M. F. Parsons, M. Kanasz-Nagy, R. Schmidt, F. Grusdt, E. Demler, D. Greif, and M. Greiner, A cold-atom Fermi-Hubbard antiferromagnet, Nature (London) **545**, 462 (2017).

[73] A. Bohrdt, D. Greif, E. Demler, M. Knap, and F. Grusdt, Angle-resolved photoemission spectroscopy with quantum gas microscopes, Phys. Rev. B **97**, 125117 (2018).